IEEE Access
Multidisciplinary | Rapid Review | Open Access Journal

Received November 25, 2019, accepted December 5, 2019, date of publication December 30, 2019,
date of current version January 22, 2020.

Digital Object Identifier 10.1109/ACCESS.2019.2963101

Robotic Biceps Exercise Machine: Hardware Using Series Elastic Actuator and Control With Disturbance Observer

KYUNGNAM KIM AND DAEHIE HONG
School of Mechanical Engineering, Korea University, Seoul 02841, South Korea

Corresponding author: Daehie Hong (dhhong@korea.ac.kr)

This work supported by the Ministry of Trade, Industry and Energy (MOTIE), South Korea, through the Industrial Technology Innovation Program under Grant 20003739.

ABSTRACT Resistance training is a popular form of exercise owing to its health-related and athletic performance benefits. Robotic exercise machines using human-robot interaction are a promising solution for designing resistance training programs that successfully achieve training gains. We propose a robotic biceps exercise machine that generates a variable resistance force profile and controls the interaction force corresponding to the profile through a range of motion of exercises. A series elastic actuator measures and controls the resistance force. A novel cascade control structure comprising an inner velocity and outer force control is presented. The inner loop disturbance on the dynamics and outer loop disturbance on the kinematics are eliminated by a disturbance observer (DOB) in each loop. The performance of the proposed force control scheme is validated by comparisons with the conventional DOB and proportional-integral (PI) control schemes. Additionally, the resistance force profile and interaction force of a conventional robotic biceps exercise machine are analyzed experimentally.

INDEX TERMS Biceps exercise, disturbance observer, human-robot interaction, robotic exercise machine, series elastic actuator, variable resistance.

I. INTRODUCTION

Resistance training is an exercise form in which muscle action is used to resist an opposing force. It is one of the most popular forms of exercise because of its health-related benefits, boosts in athletic performance, and aesthetic effects [1]–[4]. The primary effects of resistance training are improvement in muscular strength, endurance, power, and hypertrophy. To achieve these gains successfully, the resistance training plan must be designed with prudence. Choosing the type of resistance training is an important part of its design. The types of resistance training are classified as follows [5].

1) Isometric training:
   Isometric means ''same length.'' In isometric training, there is no joint angle change during muscular action. Resistance force can be generated by an immovable object, such as a wall.
2) Isokinetic training:
   Isokinetic means ''same velocity.'' Muscular action is performed as the training equipment moves at a constant velocity.
3) Isoinertial training:
   Isoinertial means ''same inertia.'' Weight induced by constant inertia and gravity generates resistance force. It is the most common type of resistance training. Free weights and resistance training machines that have circular pulleys are included in this type of resistance training.
4) Variable resistance training:
   Variable resistance implies that the resistance varies throughout the range of motion (ROM). Resistance training machines that change the moment arm of the cam and the elastic band generating resistance force according to the length of the band, are included in this type of training.

Variable resistance training is a relatively new concept compared to other types of resistance training. If the variable resistance force matches the strength curve throughout an exercise's ROM, it can induce near-maximal or maximal force throughout the ROM, resulting in maximal muscular gain [5]. Despite this possible advantage, a few in-depth studies on variable resistance training have been performed compared to the other types of resistance training [6]–[8].

The associate editor coordinating the review of this manuscript and approving it for publication was Yu-Huei Cheng.

This work is licensed under a Creative Commons Attribution 4.0 License. For more information, see http://creativecommons.org/licenses/by/4.0/

One reason for the lack of research is the absence of variable resistance training equipment that can shape resistance force profiles without difficulty. The resistance force profile of numerous commercial resistance training machines does not match the strength curve throughout the ROM [9] and it is difficult to shape the resistance force. A conventional variable resistance training equipment generates resistance force using the moment arm of the cam and constant weight. Its resistance force varies because the moment arm of the cam varies throughout the exercise's ROM. Because the cam shape of the conventional variable resistance training equipment is fixed, the variable resistance force profile is also fixed, i.e., it is not variable. ''Variable'' variable resistance training equipment enables the change in the resistance force profile, via manual rotation of the starting position of the cam using the switching handle [5]. It is possible for this equipment to switch the resistance force profile among the three major types of strength curves, namely, the bell-shaped, ascending, and descending curves. Isoinertial training with an elastic band is also a type of variable resistance training. The resistance force profile can be shaped using the point where the elastic band begins to stretch, and its elastic modulus. However, it is cumbersome to set the shape of the variable resistance force profile for a certain ROM, and the shape changes depend on the ROM.

Physical human-robot interaction (pHRI) is one of the prominent solutions for the development of variable resistance equipment by programming the resistance force and controlling interaction force. There have been numerous studies on resistance training with pHRI; however, few attempts have been made at studying variable resistance training that controls the interaction force precisely according to the desired resistance. A smart exercise machine exploited three-dimensional strength curves of the human arm and the optimization criterion of the mechanical power consumption [10], [11]. This machine did not directly shape the resistance force profile because it was automatically set by the criterion maximizing calorie consumption. In [12], a muscle-strengthening rehabilitation device using magnetorheological fluid was proposed to adjust the target resistance force profile aiming to optimize the rehabilitation effect. This device is strictly safe; however, only a concentric leg lift is available because it uses a damper to generate the resistance force. A haptic-based resistance machine proposed by our research group used an admittance control scheme using a force sensor to adjust the resistance force profile [13]. This admittance control scheme was an open-loop force control and the force error was determined by the target admittance. It had a performance limitation of precise force control because there exist upper bound of the target admittance guaranteeing stability of the system. A prototype of the series elastic resistance mechanism for exercise and rehabilitation generated variable resistance force during an exercise stroke [14]. A proportional-derivative-integral (PID) controller was applied to control the prototype, and only constant force control was implemented by maintaining a constant deflection of the spring. In [15], a muscle training robot, with a programmable exercise load, named Dynamic Dumbbell was presented. It demonstrated impressive force control performance courtesy of the series elastic actuator (SEA) with a disturbance observer (DOB). However, the actual interaction force differed from the desired resistance force because the control variable was the spring deflection between the load link and motor transmission, i.e., link inertial and frictional forces were added to the resistance force.

An SEA is a widely accepted mechanism for pHRI because of its safety and improved force control [16]–[22]. Disturbances and uncertainties have a significant impact on control performance of the SEA. Numerous researchers have studied disturbance/uncertainty estimation and attenuation techniques such as disturbance observers [23]–[26], unknown input observers [27], [28], and extended state observers [29]–[31], which have been applied to various industries. Recently, several studies on the application of a DOB to an SEA to control precise force have been conducted, and performance has been improved. Kong et al. used a proportional-derivative (PD) controller using a linear quadratic method with a DOB to obtain good torque tracking performance [32]. Oh and Kong modeled an SEA as a two-mass system, and proposed a model-based controller using a DOB with a feedforward to achieve high speed and high precision force control [33]. This SEA with DOB could be the key to developing a robotic exercise machine for variable resistance training. Most studies of SEA with DOB have focused on the control of interaction force between the SEA and the link; however, for the generation of resistance force, the interaction force between the link and human must be controlled. We focused on the force applied to humans to generate the resistance force. The main hindrance in controlling the interaction force between the link and human are disturbances on the kinematics between them. A DOB could be the solution to rejecting disturbance in kinematics. This study proposes a robotic resistance exercise machine using an SEA with a DOB for the generation of a variable resistance force pragmatically. Hardware using an SEA and a novel cascade control using a DOB to control the interaction force between the robotic arm and a human is presented. The contributions of this study are:

1) The design and construction of a robotic biceps exercise machine using an SEA to control the force applied on a human, i.e., resistance force.
2) A novel cascade control structure with DOBs designed to reject disturbances on the dynamics and kinematics.
3) The performance of generating a variable resistance force profile is validated by comparison with a conventional biceps exercise machine.

II. ROBOTIC BICEPS EXERCISE MACHINE

The robotic biceps exercise machine has one active degree of freedom joint driven by a servo motor and a harmonic

FIGURE 1. Robotic biceps exercise machine.

drive set (Fig. 1). The SEA part comprises the servo motor and harmonic drive set, a robotic arm, the elastic module, and a grip bar. The robotic arm attached to the harmonic drive and grip bar are connected by an elastic module, which includes the die spring. To control the force applied to a human, the elastic module is located just before the grip bar. This enables a more precise control of the force applied to a human in comparison with conventional SEAs, in which the actuator and elastic element are close together. The frame of the robotic biceps exercise machine was retrofitted from a conventional arm curl machine. Weight stacks on the right side of the preacher curl bench were removed and the SEA part was installed on the left side, maintaining the same rotational axis. The subject can cut off the power of the servo motor, using an emergency switch, with his/her left knee in the event of an unexpected fault. Fig. 2 represents the details of the elastic module and grip bar. The grip bar and ball bush section are connected by a wire rope. When the grip bar is pulled, the ball bushes slide along the guide axis and the two die springs are compressed, a portion of the ball bush drives the timing belt, and finally, a pulley rotates.

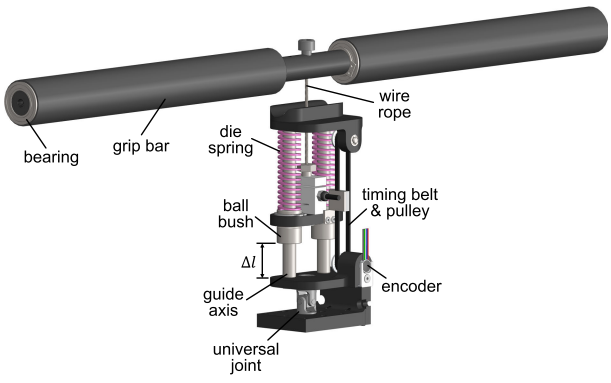

FIGURE 2. Elastic module and grip bar of robotic biceps exercise machine.

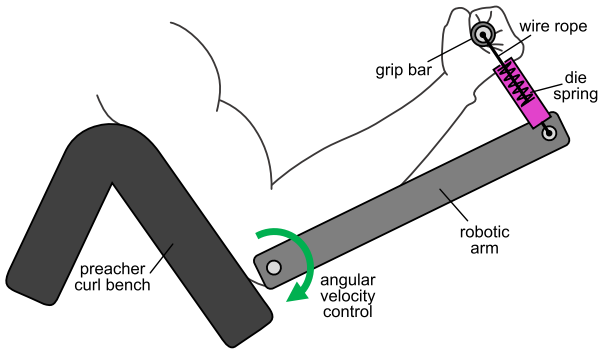

FIGURE 3. Schematic of biceps exercise using robotic biceps exercise machine.

The rotation angle of the pulley is measured by the encoder and is then converted to the driving length of the timing belt, i.e. deflection of the spring, by the arc length formula. Deflection of the spring refers to the interaction force by Hook's law. The wire rope, universal joint, and bearing in the grip bar provide passive degrees of freedom and enable the motion of the forearms to naturally fit throughout the exercise's ROM. Fig. 3 illustrates the schematic of the biceps exercise using the proposed machine. The upper arms are fixed to a preacher curl bench and the elbow joint axes coincide with the rotation axis of the robotic arm. The deflection of the spring, referred to as interaction force, can be controlled by controlling the angular velocity of the robotic arm. The hardware specifications of the robotic biceps exercise machine are summarized in Table 1.

TABLE 1. Specification of hardware.

Description	Value
gear ratio of harmonic drive	80:1
motor power	500 W
measured spring stiffness	6.41 N/mm
resolution in measurement of Δl	7.38 μm/count
maximum force by spring compression	269 N
maximum continuous force by motor torque	288 N
maximum peak force by motor torque	973 N

III. CONTROL OF ROBOTIC BICEPS EXERCISE MACHINE

Fig. 4 illustrates the kinematics model when the robotic biceps exercise machine interacts with the human forearm in

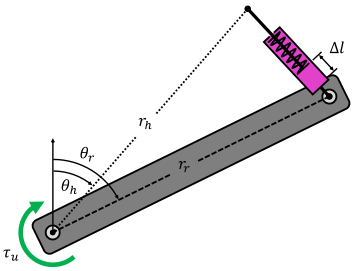

FIGURE 4. Kinematics model of the robotic arm and the human forearm.

the sagittal plane. We define the problem of generating the variable resistance force profiles as determining the motor input torque τ_u, so that Δl becomes Δl^d for varying θ_h. The significant difficulties in dealing with the problem are the disturbances and uncertainties surrounding the dynamics of the robotic arm and the kinematics. The definition of the terms used in this paper is summarised in Table 2.

TABLE 2. Nomenclature.

Δl	deflection length of the spring
Δl^d	desired deflection length of the spring
r_r	length of the robotic arm link
r_h	length of the human forearm
θ_r	angle of the robotic arm
$\dot{\theta}_r$	angular velocity of the robotic arm
$\dot{\theta}_r^d$	desired angular velocity of the robotic arm
θ_h	angle of human forearm
$C_{vel,ff}$	velocity feedforward controller
$C_{vel,fb}$	velocity feedback controller
$C_{SEA,ff}$	SEA force feedforward controller
$C_{SEA,fb}$	SEA force feedback controller
d_r	lumped disturbance on the dynamics of the robotic arm
d_k	lumped disturbance on the kinematics between the robotic arm and human forearm
$\hat{d}_k$	estimate of lumped disturbance on the kinematics between the robotic arm and human forearm
Q_r	DOB filter for velocity control
Q_k	DOB filter for SEA force control
P_r	dynamics of the robotic arm
$P_{r,n}$	nominal dynamics of the robotic arm
P_k	kinematics between the robotic arm and human forearm
$P_{k,n}$	nominal kinematics between the robotic arm and human forearm
τ_u	control input torque

We propose the cascade control structure, comprising an inner velocity control with DOB_{vel} and outer SEA force control with DOB_{SEA}. Its advantage is that it is possible to deal separately with the disturbances acting on each control, i.e., the disturbances that interfere with the velocity control are handled in the velocity control, and the disturbances that interfere with the force control are handled in the force control. The proposed control structure comprises four nested feedback loops and two feedforward controllers, as illustrated in Fig. 5. The inner velocity control is achieved by two inner loops and a feedforward controller and the outer SEA force control is achieved by two outer loops and another feedforward controller. The innermost DOB loop increases

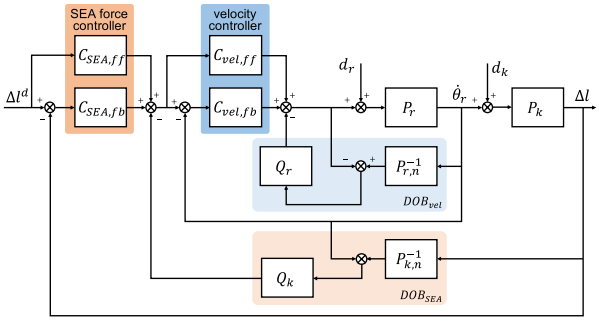

FIGURE 5. Block diagram of the cascade control structure with DOBs.

performance in the presence of disturbance, and uncertainty, of the robotic arm dynamics when the velocity controller performs velocity tracking control. The second inner feedback loop achieves velocity tracking with the velocity feedforward controller. The next DOB loop eliminates the effects of uncertainty and disturbance on the kinematics, such as the length and angular velocity of the subject's forearm when the SEA force controller performs force tracking control. The outermost feedback loop is utilized for an SEA force feedback controller that performs force tracking control with an SEA force feedforward controller.

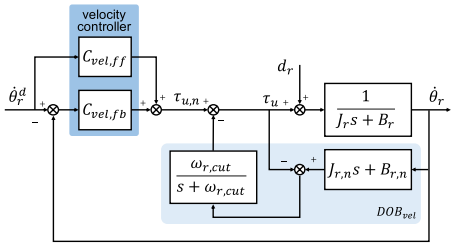

FIGURE 6. Block diagram of the inner velocity control with DOB.

Fig. 6 represents the block diagram of the inner velocity control of the robotic arm. The plant of the robotic arm P_r can be linearly modeled as $\frac{1}{J_r s+B_r}$, where the input is the force and the output is the velocity. The model variation and disturbance on the model can be lumped into disturbance d_r. The parameters, such as inertia J_r and viscous friction coefficient B_r, of the plant are uncertain, and unknown disturbances, such as gravity and spring forces, act on the plant, and interfere with the velocity control of the robotic arm. To cope with these disturbances, we employed a linear DOB [25] applied to a conventional velocity controller that comprises both feedback and feedforward controllers [24]. The DOB is named DOB_{vel} to distinguish it from the DOB that follows. The basic structure of the linear DOB comprises a nominal model and a DOB filter. Lumped disturbance on the robotic arm can be estimated by the difference between the control inputted to the plant τ_u and the calculated input torque obtained from the inverse nominal model. The estimated disturbance is subtracted after passing through the DOB filter and disturbance is rejected. The system response of the closed-loop velocity control system with DOB_{vel} in the frequency domain is

$$\begin{aligned}\dot{\theta}_r &= \frac{(C_{vel,ff}+C_{vel,fb})P_{r,n}P_r}{P_{r,n}(1+C_{vel,fb}P_r)-Q_r(P_{r,n}-P_r)}\dot{\theta}_r^d \\ &\quad + \frac{(1-Q_r)P_{r,n}P_r}{P_{r,n}(1+C_{vel,fb}P_r)-Q_r(P_{r,n}-P_r)}d_r \\ &= T_{\dot{\theta}_r,\dot{\theta}_r^d}\dot{\theta}_r^d + T_{\dot{\theta}_r,d_r}d_r. \end{aligned} \tag{1}$$

For the sake of simplicity, the variable s is omitted. $T_{\dot{\theta}_r,\dot{\theta}_r^d}$ and $T_{\dot{\theta}_r,d_r}$ refer to the transfer functions from the desired velocity input $\dot{\theta}_r^d$ and disturbance on the robotic arm d_r to the angular velocity of the robotic arm $\dot{\theta}_r$, respectively. The disturbance rejection performance of DOB_{vel} is primarily influenced by the design of the DOB filter Q_r. The DOB filter,

Q_r, is chosen as a first-order low-pass filter in the form of $\frac{\omega_{r,cut}}{s+\omega_{r,cut}}$ for simplicity of analysis. As the cuff-off frequency of Q_r approaches infinity, Q_r approaches 1. This causes the influence of disturbance on dynamics $T_{\dot{\theta}_r d^d}$ to be rejected, i.e.,

$$\lim_{\omega_{d,cut}\to\infty} T_{\dot{\theta}_r,d_r} d_r = 0. \tag{2}$$

Additionally, the velocity control system response $\dot{\theta}_r$ approaches the nominal plant response controlled by the feedback and feedforward controller, i.e.,

$$\lim_{\omega_{d,cut}\to\infty} \dot{\theta}_r = \frac{(C_{vel,ff} + C_{vel,ff})P_{r,n}}{1 + C_{vel,fb}P_{r,n}}\dot{\theta}_r^d. \tag{3}$$

This implies that the velocity-controlled uncertain plant with model parametric uncertainties and unknown disturbances behaves the same as a velocity-controlled known plant without any uncertainties and disturbances. If the feedforward velocity controller $C_{vel,ff}$ is chosen as $Q_r P_{r,n}^{-1}$ with the condition of $\omega_{r,cut} \to \infty$, $\dot{\theta}_r$ approaches $\dot{\theta}_r^d$, i.e., perfect velocity tracking is possible because it is a matter of controlling a plant ideally modeled with known parameters when the disturbances are perfectly rejected. However, in the practical implementation of the digital controller via DOB, the cut-off frequency of the DOB filter cannot increase infinitely because of the sensor noise and numerical differentiation of the digital controller.

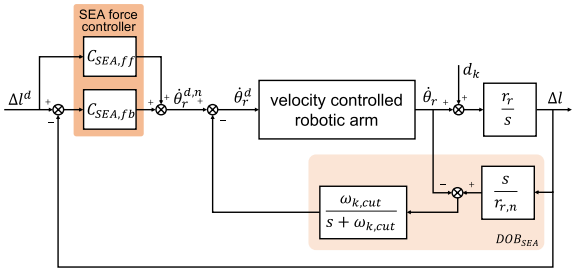

FIGURE 7. Block diagram of the outer SEA force control with DOB.

Outer SEA force control is performed using two outer loops to control the interaction force between the robotic arm and the subject's hands. The block diagram of the outer SEA force control is depicted in Fig. 7. The interaction force between the robot arms and human hands is transformed from spring deflection Δl by Hook's law. Therefore, the control problem of the interaction force between the robot arms and human hands turns into the control problem of spring deflection Δl. This is one of the significant benefits of using an SEA for interaction force control. The feedback and feedforward controllers of an SEA force control generate the reference velocity $\dot{\theta}_r^{d,n}$ required to reduce the error of spring deflection corresponding to the error of interaction force. The kinematic structure of the robotic arms connected to human hands by a spring is modeled as a triangular configuration, as illustrated in Fig. 4. In this triangular configuration, the major obstacles to controlling interaction force using an internal velocity controller are as follows: a nonlinear relationship between the robotic arm angle and spring deflection, uncertain kinematic parameters, such as the length of the human forearm r_r, and variations in the human joint angles θ_r. We propose DOB_{SEA} to cope with disturbances on the kinematics. The primary idea of the proposed control scheme is to use a DOB to eliminate the disturbances on the kinematics model so that the nonlinear kinematics act as a nominal linear kinematics model and applies a linear SEA force controller to the nominal model. The kinematics of the robot's angular velocity input and spring deflection output can be linearly modeled with lumped disturbance as follows.

$$\Delta l = P_k\dot{\theta}_r + P_k d_k. \tag{4}$$

Controlling the spring deflection is straightforward, provided that the internal velocity controller is perfect and the kinematics model is linear and has known parameters. DOB_{SEA} eliminates the disturbance on kinematics in the loop just outside the velocity controller, making the desired reference velocity $\dot{\theta}_r^{d,n}$, which is the output of the SEA force controller, behave linearly with the spring deflection Δl. The response of the spring deflection Δl to the reference velocity $\dot{\theta}_r^{d,n}$ input in the frequency domain is

$$\begin{aligned}\Delta l &= \frac{T_{\dot{\theta}_r,\dot{\theta}_r^d} P_{k,n} P_k}{P_{k,n} - Q_k T_{\dot{\theta}_r,\dot{\theta}_r^d}(P_{k,n} - P_k)}\dot{\theta}_r^{d,n} \\ &\quad + \frac{T_{\dot{\theta}_r,d_r} P_{k,n} P_k}{P_{k,n} - Q_k T_{\dot{\theta}_r,\dot{\theta}_r^d}(P_{k,n} - P_k)} d_r \\ &\quad + \frac{(1 - T_{\dot{\theta}_r,\dot{\theta}_r^d} Q_k) P_{k,n} P_k}{P_{k,n} - Q_k T_{\dot{\theta}_r,\dot{\theta}_r^d}(P_{k,n} - P_k)} d_k \\ &= T_{\Delta l,\dot{\theta}_r^{d,n}}\dot{\theta}_r^{d,n} + T_{\Delta l,d_r} d_r + T_{\Delta l,d_k} d_k.\end{aligned} \tag{5}$$

$T_{\Delta l,\dot{\theta}_r^{d,n}}$, $T_{\Delta l,d_r}$, and $T_{\Delta l,d_k}$ refer to the transfer functions from the output of the SEA force controller $\dot{\theta}_r^{d,n}$, disturbance on the dynamics of the robotic arm d_r, and disturbance on the kinematics between the robotic arm and human forearm d_k, respectively, to the spring deflection Δl. The DOB filter Q_k is chosen as a first-order low-pass filter in the form of $\frac{\omega_{k,cut}}{s+\omega_{k,cut}}$. If the internal velocity controller is almost perfect, with an infinite cut-off frequency Q_k, i.e., $T_{\dot{\theta}_r\dot{\theta}_r^d} \approx 1$, $T_{\dot{\theta}_r d_r} \approx 0$, and $T_{\Delta l,d_k} \approx 0$, then the the influence of the disturbance on kinematics $T_{\Delta l,d_k} d_k$ to be almost rejected, i.e.,

$$T_{\Delta l,d_k} d_k \approx 0. \tag{6}$$

And the response of the spring deflection Δl will be

$$\Delta l \approx P_{k,n}\dot{\theta}_r^{d,n}. \tag{7}$$

This implies that the input to the velocity controller and deflection of the spring referred to as interaction force is linear, which makes the control of the interaction force between the robotic arms and human hands straightforward. The feedback and feedforward controllers for SEA force control are employed in the outermost loop. The total closed-loop system

response Δl for Δl^d in the frequency domain is

$$\Delta l = \frac{(C_{SEA,ff} + C_{SEA,fb})T_{\Delta l,\dot{\theta}_r^{d,n}}}{1 + C_{SEA,fb}T_{\Delta l,\dot{\theta}_r^{d,n}}}\Delta l^d + \frac{T_{\Delta l,d_r}}{1 + C_{SEA,fb}T_{\Delta l,\dot{\theta}_r^{d,n}}}d_r + \frac{T_{\Delta l,d_k}}{1 + C_{SEA,fb}T_{\Delta l,\dot{\theta}_r^{d,n}}}d_k. \quad (8)$$

If the feedforward SEA force controller $C_{SEA,ff}$ is chosen as $Q_k P_{r,n}^{-1}$, with an infinite cut-off frequency of Q_k and the almost perfect velocity controller, i.e., $T_{\Delta l,\Delta l^d} \approx 1$, $T_{\Delta l,d_r} \approx 0$, and $T_{\Delta l,d_k} \approx 0$, then, the response of the spring deflection Δl approaches Δl^d. This indicates that the force tracking performance is improved by eliminating the disturbances on the kinematics which are significant obstacles in controlling the interaction force.

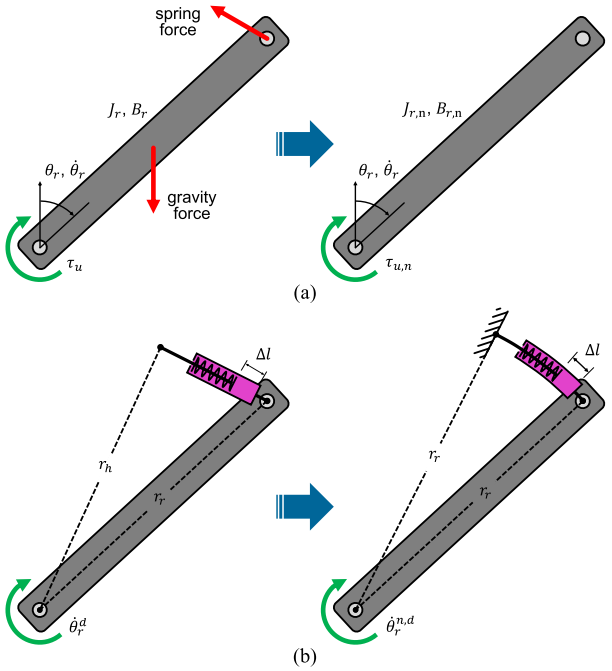

FIGURE 8. Intuitive representation of the cascade control structure with DOBs. (a) Inner velocity control with DOB; (b) outer SEA force control with DOB.

Fig. 8 represents an intuitive explanation of the proposed cascade DOB. The DOB_{vel} of the inner loop velocity control makes the uncertain dynamics of the robotic arm under disturbance act similar to known dynamics without disturbance, i.e.,disturbances, such as gravity, spring force, and parametric uncertainties are rejected and the design of the inner loop velocity control is based on nominal dynamics without disturbances (Fig. 8 (a)). DOB_{SEA} of the outer loop SEA force control rejects the disturbances acting on the kinematics between the robotic and forearms, which turn the kinematics into a circular sector with nominal parameters (Fig. 8 (b)). The design of the outer loop SEA force control is based on the nominal kinematics. The cascade control structure with DOBs eliminate the disturbances on the dynamics and kinematics where each disturbance occurs.

IV. EXPERIMENT

A. CONSTANT RESISTANCE FORCE PROFILE

The performance of the proposed control scheme in generating a constant resistance force was validated when a subject performed three repetitions of a biceps exercise, in which the desired forces were 50 and 100 N. 100 N was the approximate weight the subject could perform exercise movements 20 times in succession with proper motion, i.e., 20 repetition maximum. The arbitrarily set lighter weight was 50 N at half of 100 N. A biceps exercise movement comprises concentric muscle action (CON) and eccentric muscle action (ECC). CON movements occur when the biceps shorten against external load and elbow flexion occurs. An example is lifting a weight. ECC movements occur when the biceps lengthen under external load in a controlled manner and elbow extension occurs. An example is lowering a weight. The ROM of the biceps exercise was set at 135° in the human elbow rotation coordinate, and 0° where the forearms were fully extended on the preacher bench tilted at 55° from the ground. In all experiments, the subject was required to perform a periodic motion of a 1 s CON movement and a 2 s ECC movement in all the experiments. With a metronome set to beat for every 1 second and 1 accent beat for every 3 beats, the subject attempted to complete a CON movement in each accent beat for consistent periodic movement. Three control schemes for generating a constant force profile were evaluated: C_{SEA} with DOB_{SEA} and C_{vel} with DOB_{vel}, which reject the disturbance on kinematics and dynamics (KIN); C_{vel} with DOB_{vel}, which rejects the disturbance on dynamics (DYN); PI force control, which is a conventionally adopted in force control (PI). In the DYN control scheme, DOB_{vel} and $C_{vel,ff}$ were added to the PI control scheme with the same PI control parameter. In the KIN control scheme, DOB_{SEA} and $C_{SEA,ff}$ were added to the DYN control scheme with the same DYN control parameter. The control parameters were empirically set in a range that satisfies the robust stability of the DOB proposed in [35]. The control parameters used in the experiments are summarized in Table 3. The inertia term of the velocity feedforward controller is excluded because it is too noisy to be used as the second derivative of the interaction force.

TABLE 3. Control parameters.

	KIN	DYN	PI
$C_{vel,fb}$	$5(1+\frac{1}{0.6s})$	$5(1+\frac{1}{0.6s})$	$5(1+\frac{1}{0.6s})$
$C_{SEA,fb}$	$2(1+\frac{1}{0.6s})$	$2(1+\frac{1}{0.6s})$	$2(1+\frac{1}{0.6s})$
$P_{r,n}^{-1}$	$0.01s+0.5$	$0.01s+0.5$	-
Q_r	$\frac{100}{s+100}$	$\frac{100}{s+100}$	-
$C_{vel,ff}$	0.5	0.5	-
$P_{k,n}^{-1}$	$\frac{s}{0.32}$	-	-
Q_k	$\frac{500}{s+500}$	-	-
$C_{SEA,ff}$	$\frac{s}{0.32}\frac{500}{s+500}$	-	-

Fig. 9 depicts the angle of the robotic arm with respect to time when the subject performs the biceps exercise movement. In all the cases, the direction of the angular velocity changes from positive to negative, changing from CON to ECC around 1, 4, and 7 s and vice versa around 0, 3, and 6 s. This implies that the subject has made consistent periodic movements in all the trials.

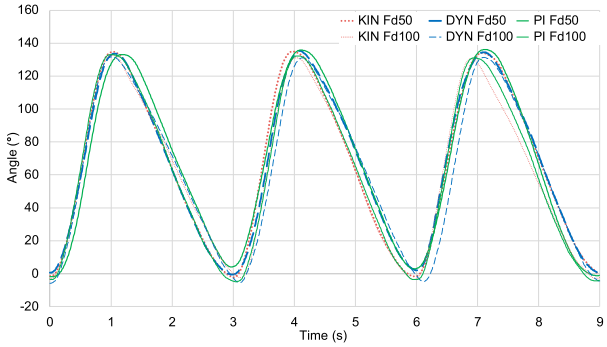

FIGURE 9. Angle of robotic arm during constant desired force experiments.

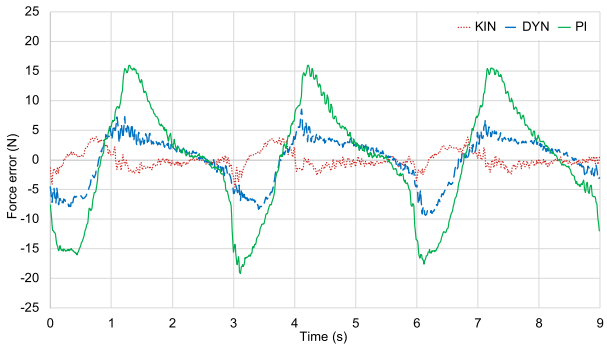

FIGURE 10. Error of interaction force when the desired force is 50 N.

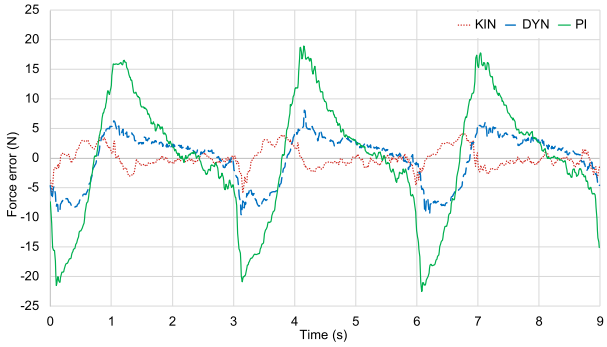

FIGURE 11. Error of interaction force when the desired force is 100 N.

Fig. 10 and 11 depict the force tracking error of the three control schemes when the desired force is 50 N and 100 N, respectively. Both cases have similar patterns regardless of the magnitude of the desired force. The peak force error and root mean square error (RMSE) of each control scheme in both cases are summarized in Table 4. Among the three control schemes, the KIN control scheme exhibits the least peak force error and RMSE. The peak force errors of the PI and DYN control schemes occur immediately after the change in direction of the angular velocity. The structure of the PI control scheme is comprised of two loops: an outer loop that feeds back the spring deflection and generates the desired velocity by $C_{SEA,fb}$, and an inner loop that feeds back the angular velocity and generates the control input torque by $C_{vel,fb}$. The linear PI controllers is applied for $C_{SEA,fb}$ and $C_{vel,fb}$, which induce a zero steady state error; however, a period of time is required before the rejection of disturbance begins because the integral action accumulates errors linearly over time to eliminate the disturbance. Therefore, the PI control scheme is not sufficiently equipped to reject rapidly varying disturbances, such as change in direction of velocity on the SEA force control and spring force on the robotic arm velocity control. Control schemes with DOB are expected to have a faster error rejection response than the PI control scheme, because it does not wait for an accumulation of errors but estimates the disturbance for the nominal plant model and eliminates them promptly. The force-tracking performance of the DYN control scheme is improved by using DOB_{vel} and feedforward controller for the internal velocity controller. However, the DYN control scheme requires a period of time to reduce the force error when rapidly varying disturbances act on the kinematics, such as change in the velocity direction of the subject's limb because the outer SEA force control uses only a PI controller. The main cause of the force error in the outer SEA force loop is disturbances on the kinematics such as human motion. The KIN control scheme exploited DOB_{SEA} to estimate disturbances on the kinematics from spring deflection, robotic arm velocity, and nominal kinematics model, i.e., $\hat{d}_k = Q_k(P_{r,n}^{-1}\Delta l - \dot{\theta}_r)$; the estimated disturbance was subtracted promptly. The physical meaning of disturbances on the kinematics is the angular velocity of the subject's forearm. Fig. 12 depicts the estimate for disturbance on the kinematics exploited in the KIN control scheme when the desired force is 100 N. These values were calculated using Δl and $\dot{\theta}_r$ in each sampling time and were then promptly subtracted from the desired velocity command. Estimated disturbance had peak values around 0.5, 3.5, and 6.5 s. These times correspond to the peak times of the force error in DYN control scheme without DOB_{SEA}. This means improvement of force control performance by DOB_{SEA}. Additionally, similar force tracking performance can be expected provided that a subject performs similar periodic movements with another subject because DOB_{SEA} estimate disturbance by the movements.

TABLE 4. RMSE, peak force error.

	desired force 50 N		desired force 100 N	
	RMSE (N)	peak error (N)	RMSE (N)	peak error (N)
KIN	1.45	4.54	1.70	6.38
DYN	4.01	9.36	4.18	9.59
PI	9.25	19.15	9.99	22.55

B. VARIABLE RESISTANCE FORCE PROFILE

We validated the performance of the robotic biceps exercise machine to generate a variable resistance force compared

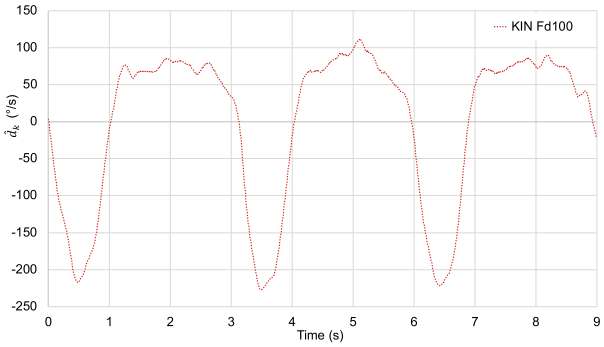

FIGURE 12. Estimate of lumped disturbance on kinematics when the desired force is 100 N.

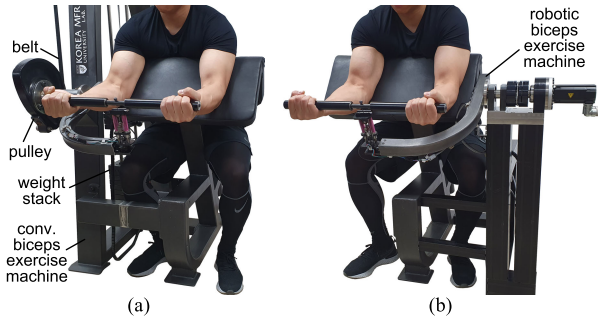

FIGURE 13. Resistance force profile and interaction force experiment. (a) Conventional biceps exercise machine; (b) robotic biceps exercise machine.

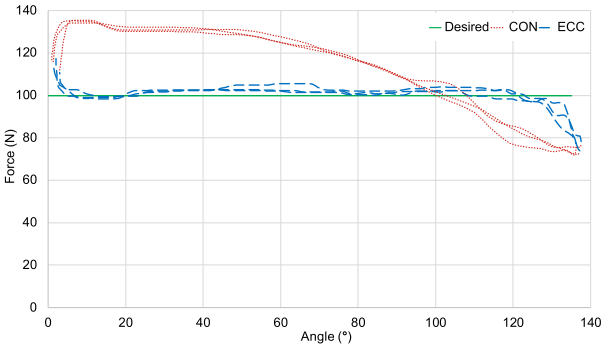

FIGURE 14. Constant resistance force profile and interaction force with respect to angle of conventional biceps machine.

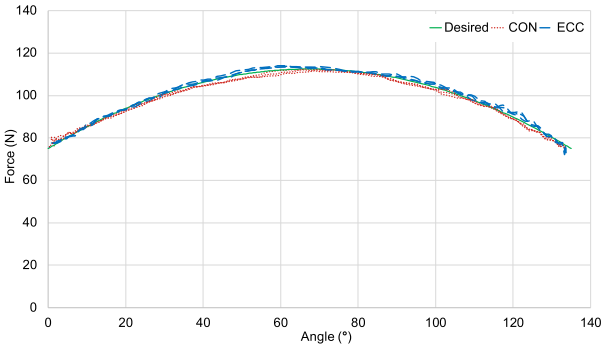

FIGURE 15. Quadratic resistance force profile and interaction force with respect to angle of robotic biceps machine.

to that of a conventional biceps exercise machine when the subject performs the same movement as that in the constant resistance force profile experiment (Fig. 13). The conventional biceps exercise machine uses the same preacher bench, robotic arm, grip bar, and rotation axis as the robotic biceps exercise machine, with the robotic arm positioned to the right side of the subject. The resistance force is generated by weight stacks connected by a belt to a pulley. The key factors that determine the resistance force profile are the moment arm of the pulley and weight of the weight stack. The moment arm of the pulley was constant, and the weight of the weight stack was set so that in a static condition, the interaction force was 100 N at the position where the forearms are fully extended, i.e., the nominal resistance force profile was made constant. Fig. 14 depicts the interaction forces with respect to the angle during three repetitions with the conventional biceps exercise machine. Due to the inertia of the weight stack, more interaction force is generated during acceleration when changing from ECC to CON, and less interaction force is generated during deceleration when changing from CON to ECC. The interaction force is significantly deviate from the nominal resistance force according to the subject's motion.

The variable resistance force profile was generated by setting the desired force as a quadratic function with 100 N at each end and a 150% peak of the endpoint value at the midpoint of the ROM. The KIN control scheme was also employed with the same control parameters. Fig.15 depicts the desired force and interaction force with respect to the robotic arm angle. The interaction force is larger than the desired value in a narrow section near 0° where ECC turns into CON, because the angular velocity of the elbow joint changes direction and the angle increases; however, the angular velocity of the robotic arm cannot respond at that instant and the spring is compressed more than the desired spring deflection. The reason for the smaller interaction force near 135° is the reciprocal of that near 0°. However, the proposed controller immediately responded to the change in velocity direction and maintained the interaction force at the desired force value. The RMS force error was 1.25 N and peak force error was 4.71 N during the three repetitions of the biceps exercise.

Two types of time-dependent resistance profiles were generated: a constant-ascent profile, and a constant-descent profile. The KIN control scheme was also utilized with the same control parameters. The desired force of the constant-ascent profile began at 70 N and maintained the values were maintained for 3 s. Then, the desired force increased by 5 N per second for the remaining 6 s. The desired force of the constant-descent profile began at 100 N and the value was maintained for 3 s. Subsequently, the desired force decreased by 5 N per second for the remaining 6 s. The constant-ascent profile and interaction forces are shown in Fig.16. The patterns of force errors are similar to that of the constant desired force, i.e., the force error increased when the direction of angular velocity of the elbow changed and

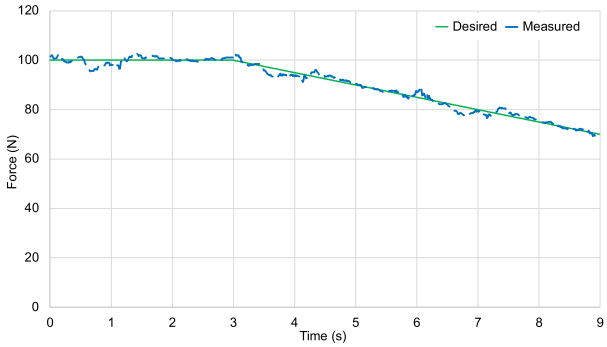

FIGURE 16. Constant-ascent resistance force profile and interaction force with respect to angle of robotic biceps machine.

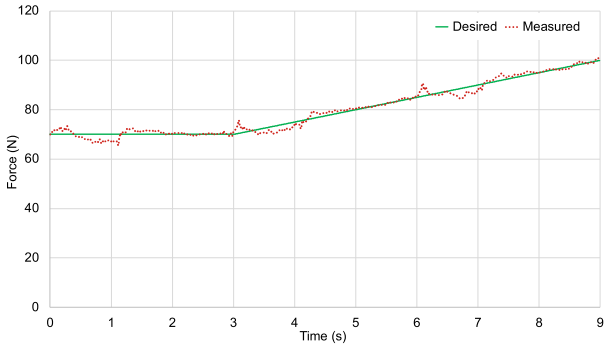

FIGURE 17. Constant-descent resistance force profile and interaction force with respect to angle of robotic biceps machine.

decreased immediately. The RMS force error was 1.53 N and the peak force error was 5.27 N during the three repetitions. Fig.17 depicts the constant-descent profile and interaction forces. The force error also has similar patterns with the constant desired force in the case of the constant-descent profile. The RMS force error was 1.45 N and the peak force error was 4.72 N. The time-varying resistance force profile means that the interaction force can be adjusted in the middle of the repetition through considerations of user status such as fatigue, which is not realizable in conventional resistance training equipment.

V. CONCLUSION

This study proposed a robotic biceps exercise machine to generate a variable resistance force profile and control the interaction force corresponding to the profile. The hardware of the robotic biceps exercise machine was retrofitted from a conventional biceps exercise machine and comprised an SEA to measure and control the interaction force for generating the resistance force. We proposed a cascade control structure for control of the interaction force in the presence of disturbances and uncertainties, which comprised an inner velocity control with DOB_{vel} and outer SEA force control with DOB_{SEA}. DOB_{vel} rejects the disturbance on the dynamics of the robotic arm and causes the robotic arm to behave as nominal dynamics. DOB_{SEA} rejects the disturbance on the kinematics between the robotic arm and the subject's forearms and causes the kinematics to behave as linear nominal kinematics. The performance of constant interaction force control was validated by the comparison with the conventional control scheme, and the proposed control scheme was superior to the conventional control scheme in terms of RMSE and peak force error. The measured interaction force and nominal resistance force profile of the conventional biceps exercise machine did not match because the interaction force was affected by the motion dependent force, such as the inertial force of the weight stack. By contrast, they were matched in the robotic biceps exercise machine, because this machine automatically controls the interaction force to the desired resistance force regardless of the motion of the human forearms. The performance of the interaction force control when the variable resistance force profile was quadratic with respect to the angle was experimentally verified. Future research is necessary to evaluate the effects of training using robotic exercise machines and to investigate the performance and stability of the cascade control using DOBs. The hardware, using an SEA and the control scheme, can be applied to robotic exercise machines that generate variable resistance force profiles and control interaction force programmatically.

ACKNOWLEDGMENT

K. Kim would like to thank Prof. Kyoungmo Jung for his invaluable advice and encouragement.

REFERENCES

[1] R. W. Braith and K. J. Stewart, "Resistance exercise training—Its role in the prevention of cardiovascular disease," *Circulation*, vol. 113, no. 22, pp. 2642–2650, Jun. 2006.
[2] M. R. Deschenes and W. J. Kraemer, "Performance and physiologic adaptations to resistance training," *Amer. J. Phys. Med. Rehabil.*, vol. 81, pp. S3–S16, Nov. 2002.
[3] W. J. Kraemer and N. A. Ratamess, "Hormonal responses and adaptations to resistance exercise and training," *Sports Med.*, vol. 35, no. 4, pp. 339–361, 2005.
[4] D. W. Dunstan, R. M. Daly, N. Owen, D. Jolley, M. De Courten, J. Shaw, and P. Zimmet, "High–intensity resistance training improves glycemic control in older patients with type 2 diabetes," *Diabetes Care*, vol. 25, no. 10, pp. 1729–1736, Oct. 2002.
[5] S. J. Fleck and W. J. Kraemer, "Types of strength training," in *Designing Resistance Training Programs*, 4th ed. Champaign, IL, USA: Human Kinetics, 2014, pp. 15–44.
[6] S. Walker, R. S. Taipale, K. Nyman, W. J. Kraemer, and K. Häkkinen, "Neuromuscular and hormonal responses to constant and variable resistance loadings," *Med. Sci. Sports Exerc.*, vol. 43, no. 1, pp. 26–33, Jan. 2011.
[7] S. Walker, H. Peltonen, J. Avela, and K. Häkkinen, "Kinetic and electromyographic analysis of single repetition constant and variable resistance leg Press actions," *J. Electromyogr. Kinesiol.*, vol. 21, no. 2, pp. 262–269, Apr. 2011.
[8] S. J. Aboodarda, J. George, A. H. Mokhtar, and M. Thompson, "Muscle strength and damage following two modes of variable resistance training," *J. Sports Sci. Med.*, vol. 10, no. 4, pp. 635–642, Dec. 2011.
[9] J. Folland and B. Morris, "Variable-cam resistance training machines: Do they match the angle–torque relationship in humans?" *J. Sports Sci.*, vol. 26, no. 2, pp. 163–169, Jan. 2008.
[10] P. Li and R. Horowitz, "Control of smart exercise machines. I. Problem formulation and nonadaptive control," *IEEE/ASME Trans. Mechatronics*, vol. 2, no. 4, pp. 237–247, Dec. 1997.
[11] P. Y. Li and R. Horowitz, "Control of smart exercise machines. II. Self-optimizing control," *IEEE/ASME Trans. Mechatronics*, vol. 2, no. 4, pp. 248–258, Dec. 1997.

[12] S. Dong, K.-Q. Lu, J. Sun, and K. Rudolph, "Adaptive force regulation of muscle strengthening rehabilitation device with magnetorheological fluids," *IEEE Trans. Neural Syst. Rehabil. Eng.*, vol. 14, no. 1, pp. 55–63, Mar. 2006.
[13] J. Park, K. Kim, and D. Hong, "Haptic-based resistance training machine and its application to biceps exercises," *Int. J. Precis. Eng. Manuf.*, vol. 12, no. 1, pp. 21–30, Feb. 2011.
[14] K. G. Gim and D. W. Hong, "Design of a series elastic resistance mechanism for exercise and rehabilitation," in *Proc. IEEE-RAS 16th Int. Conf. Humanoid Robots (Humanoids)*, Nov. 2016, pp. 1239–1244.
[15] C. Lee and S. Oh, "Dynamic dumbbell—novel muscle training robot with programmable exercise load," in *Proc. IEEE/RSJ Int. Conf. Intell. Robots Syst. (IROS)*, Oct. 2018, pp. 7648–7653.
[16] G. Pratt and M. Williamson, "Series elastic actuators," in *Proc. IEEE/RSJ Int. Conf. Intell. Robots Syst. Hum. Robot Interact. Cooperat. Robots*, Nov. 2002, pp. 399–406.
[17] J. Pratt, B. Krupp, and C. Morse, "Series elastic actuators for high fidelity force control," *Ind. Robot.*, vol. 29, no. 3, pp. 234–241, Jun. 2002.
[18] H. Yu, S. Huang, G. Chen, Y. Pan, and Z. Guo, "Human–robot interaction control of rehabilitation robots with series elastic actuators," *IEEE Trans. Robot.*, vol. 31, no. 5, pp. 1089–1100, Oct. 2015.
[19] H. Vallery, J. Veneman, E. Van Asseldonk, R. Ekkelenkamp, M. Buss, and H. Van Der Kooij, "Compliant actuation of rehabilitation robots," *IEEE Robot. Autom. Mag.*, vol. 15, no. 3, pp. 60–69, Sep. 2008.
[20] S. Li, J. Li, G. Tian, and H. Shang, "Stiffness adjustment for a single–link robot arm driven by series elastic actuator in muscle training," *IEEE Access*, vol. 7, pp. 65029–65039, 2019.
[21] M. I. Awad, D. Gan, I. Hussain, A. Az-Zu'bi, C. Stefanini, K. Khalaf, Y. Zweiri, J. Dias, and L. D. Seneviratne, "Design of a novel passive binary–controlled variable stiffness joint (BpVSJ) towards passive haptic interface application," *IEEE Access*, vol. 6, pp. 63045–63057, 2018.
[22] K. Kim and Y. S. Lee, "Implementation of mass–independent impedance control for RFSEA using a linkage arm," *IEEE Access*, vol. 7, pp. 104823–104832, 2019.
[23] K. Ohnishi, M. Shibata, and T. Murakami, "Motion control for advanced mechatronics," *IEEE/ASME Trans. Mechatronics*, vol. 1, no. 1, pp. 56–67, Mar. 1996.
[24] E. Sariyildiz and K. Ohnishi, "On the explicit robust force control via disturbance observer," *IEEE Trans. Ind. Electron.*, vol. 62, no. 3, pp. 1581–1589, Mar. 2015.
[25] J. Zhang, X. Liu, Y. Xia, Z. Zuo, and Y. Wang, "Disturbance observer–based integral sliding–mode control for systems with mismatched disturbances," *IEEE Trans. Ind. Electron.*, vol. 63, no. 11, pp. 7040–7048, Nov. 2016.
[26] B. Xu, F. Sun, Y. Pan, and B. Chen, "Disturbance observer based composite learning fuzzy control of nonlinear systems with unknown dead zone," *IEEE Trans. Syst., Man, Cybern. Syst.*, vol. 47, no. 8, pp. 1854–1862, Aug. 2017.
[27] J. Na, A. S. Chen, G. Herrmann, R. Burke, and C. Brace, "Vehicle engine torque estimation via unknown input observer and adaptive parameter estimation," *IEEE Trans. Veh. Technol.*, vol. 67, no. 1, pp. 409–422, Jan. 2018.
[28] Z. Gao, X. Liu, and M. Chen, "Unknown input observer based robust fault estimation for systems corrupted by partially–decoupled disturbances," *IEEE Trans. Ind. Electron.*, vol. 63, no. 4, pp. 2537–2547, Apr. 2016.
[29] L. Sun, Y. Zhang, D. Li, and K. Y. Lee, "Tuning of active disturbance rejection control with application to power plant furnace regulation," *Control Eng. Pract.*, vol. 92, Nov. 2019, Art. no. 104122.
[30] L. Sun, J. Shen, Q. Hua, and K. Y. Lee, "Data-driven oxygen excess ratio control for proton exchange membrane fuel cell," *Appl. Energy*, vol. 231, pp. 866–875, Dec. 2018.
[31] S. Li, J. Yang, W.-C. Chen, and X. Chen, "Generalized extended state observer based control for systems with mismatched uncertainties," *IEEE Trans. Ind. Electron.*, vol. 59, no. 12, pp. 4792–4802, Dec. 2012.
[32] K. Kong, J. Bae, and M. Tomizuka, "Control of rotary series elastic actuator for ideal force-mode actuation in human–robot interaction applications," *IEEE/ASME Trans. Mechatronics*, vol. 14, no. 1, pp. 105–118, Feb. 2009.
[33] S. Oh and K. Kong, "High–precision robust force control of a series elastic actuator," *IEEE/ASME Trans. Mechatronics*, vol. 22, no. 1, pp. 71–80, Feb. 2017.
[34] S. Li, J. Yang, W.-H. Chen, and X. Chen, "Linear disturbance estimator," in *Disturbance Observer Based Control: Methods and Applications*. Boca Raton, FL, USA: CRC Press, 2016, pp. 27–41.
[35] H. Shim and N. H. Jo, "An almost necessary and sufficient condition for robust stability of closed-loop systems with disturbance observer," *Automatica*, vol. 45, no. 1, pp. 296–299, Jan. 2009.

KYUNGNAM KIM received the B.S. degree in mechanical engineering from Korea University, Seoul, South Korea, in 2008, where he is currently pursuing the Ph.D. degree in mechanical engineering.

His research interests include physical human–robot interaction, robust control, and biomechanics.

DAEHIE HONG received the B.S. and M.S. degree from the School of Mechanical Engineering, Korea University, Seoul, South Korea, in 1985 and 1987, respectively, and the Ph.D. degree from the Department of Mechanical and Aerospace Engineering, University of California at Davis, Davis, USA, in 1994.

He is currently a Professor with the School of Mechanical Engineering, Korea University. His research interests include manufacturing automation, precision machine design and control, field robotics, and autonomous car systems.